Physica Scripta

RECEIVED
3 May 2022

REVISED
18 August 2022

ACCEPTED FOR PUBLICATION
20 September 2022

PUBLISHED
12 October 2022

PAPER

Perturbation based analytical and numerical solutions of non-Newtonian differential equation during reverse roll coating process under lubrication approximation theory

Fateh Ali[1], **Yanren Hou**[1,*], **Muhammad Zahid**[2], **M A Rana**[3], **Poom Kumam**[4,5], **Marya Kanwal**[6] and **Kanokwan Sitthithakerngkiet**[7]

[1] School of Mathematics & Statistics, Xi'an Jiaotong University, Xi'an, People's Republic of China
[2] Department of Mathematics, COMSATS University Islamabad, Abbottabad, Pakistan
[3] Department of Mathematics & Statistics, Riphah International University, Islamabad, Pakistan
[4] Center of Excellence in Theoretical and Computational Science (TaCS-CoE) & KMUTTFixed Point Research Laboratory, Room SCL 802 Fixed Point Laboratory, Science Laboratory Building, Departments of Mathematics, Faculty of Science, King Mongkut's University of Technology Thonburi (KMUTT), 126 Pracha-Uthit Road, Bang Mod, Thung Khru, Bangkok 10140, Thailand
[5] Department of Medical Research, China Medical University Hospital, China Medical University, Taichung 40402, Taiwan
[6] College of Mechanical Enginering & Applid Electonic Technology, Beijing University of Technology, Beijing, People's Republic of China
[7] Intelligent and Nonlinear Dynamic Innovations Research Center, Department of Mathematics, Faculty of Applied Science, King Mongkut's University of Technology North Bangkok (KMUTNB), 1518, Wongsawang, Bangsue, Bangkok 10800, Thailand
[*] Authors to whom any correspondence should be addressed.

E-mail: yrhou@mail.xjtu.edu.cn **and** poom.kum@kmutt.ac.th

Keywords: reverse roll coating, jhonson-segalman fluid, lubrication approximation theory, perturbation method, numerical method

Abstract

Reverse roll coating process are utilized for the purpose of applying a coating to a substrate or web by utilising different rollers in order to get the required coated surface. As a result of this, reverse roll coating process have found applications in a wide variety of industries, such as those dealing with food and medicine, electronic components, optical and LCD devices, and optical products. The main objective of this paper is to develop the mathematical formulation for the coating of thin film for an incompressible isothermal viscoelastic fluid between two reversely rotating rolls. Through the use of an appropriate dimensionless parameter, Non-dimensional nonlinear ordinary differential equations (ODEs) are derived from governing partial differential equations (PDEs). LAT (lubrication approximation theory) simplifies the dimensionless equations of fluid motion. The expressions for velocity of flow, pressure gradient and flow rate is obtained analytically by using regular perturbation method, while numeric solution of some mechanical parameters such as power input, coating thickness, roll separation force and separation points are calculated. The numerical validation of the analytical solution of the fundamental model of nonlinear constitutive flow laws is done in the Maple environment using the numeric technique which is based on finite difference method. The influence of numerous non-Newtonian parameters such as velocities ratio and Weissenberg number on velocity profiles, pressure gradient, power input, roll separation force, separation points and coating thickness of a non-Newtonian Johnson–Segalman (JS) fluid are explored via graphically and in tabular form. The outcomes demonstrate that on increasing the Weisenberg number and velocities ratio, the coating thickness on web is decreases. For the numerous values of velocities ratio, it is important to note that separation points shifted towards the nip region. In addition, the non-Newtonain parameter have signifcant impact on power input and roll separating force. The maximum coating thickness that is 1.0927 has been observed at the value of separation poin 0.9620. Hence, these factors may help in an efficient coating process and improve the substrate life.

Nomenclature

$U_r\left(\frac{m}{s}\right)$	Peripheral velocity of the reverse roll

$U_f\left(\frac{m}{s}\right)$	Peripheral velocity of forwarding roll
$R(m)$	The radius of each roll
$k=\frac{U_r}{U_f}$	Velocities ratio
$\rho\left(\frac{\mathrm{kg}}{\mathrm{m}^3}\right)$	Fluid density
H_0	Half of the nip separation
$H_r(m)$	The thickness of the coating on reverse roll
$H_f(m)$	The thickness of the coating on the forwarding roll
$\upsilon=\frac{H_f}{H_r}$	Coating thickness
$\Upsilon=\frac{H_0}{H_r}$	Ratio of the half of the nip separation to the coating thickness on the reverse roll
λ	Dimensionless flow rate

1. Introduction

Fluid and different types of polymer coatings are utilized on surfaces in various industries for instance, the metal and fabric sheets through protective, decorative and enhancing materials, paper board and paper making, cellulosic film, printing, books and magazines, x-ray films, plastic films, magnetic tapes for audio, video and computer use etc Basically, the procedure in which a fluid or any material layer is sequentially applied on a moving sheet is known as coating. The moving sheet is termed as web/substrate that is to be coated. Several methods are established for coating. Some frequently used systems are reverse roll coating, forward roll coating, metering roll coating, roll over web coating, kiss roll coating, extrusion coating, withdrawal coating, blade coating and free coating.

Roll coating is a system in which the substrate is enfolded around one roll and the fluid is fed to the nip through a second roll. The suspended fluid from the nip region splits up into two streams. The fluid adhering to the substrate generates the coated layer and the stream at the exposed roll is eliminated or recycled. Usually, the rolling elements permit the apparent application of liquid coating onto the web with a good degree of control over the coating layer thickness [1–3]. To obtain the fluid layer, numerous of factors are substantial including nature of surface, rheology of liquid, coating thickness, speed of web and coating uniformity etc [4, 5]. The significant factor for thickness and consistency of sheet is fluid flow. The thickness of coating layer usually hinges on the gap among the rolls with their speeds. Mostly, the radii of two rolls are smaller than the nip distance between both rotating rolls. The web and the rolls move in conflicting direction for reverse roll coating nevertheless both rolls at the nip move in same direction for forward roll coating [6–8].

Usually, the thickness and uniformity of the liquid sheet is required in coating. The main problem with roll coating devices is the inception of surface instabilities that are necessary to eliminate for obtaining the smooth surface layer as observed by several researchers [9, 10] for Newtonian fluids. The numerical approach through finite elements method was established by Chandio and Webster [11] for the analysis of transient instabilities in case of reverse roll coating. They noticed that the increase in foil speed increases the flow instabilities rather than the roll speed. The reverse roll coating for flow instabilities comprising on cascading and ribbing was presented by Coyle *et al* [12]. They adopted the finite element method for experimental outcomes to clarify the essential fluid properties. Hinter Maier and White *et al* [13] adopted the lubrication technique for analysis of water flow among two rolls and attained the outcomes those were compatible by their own experimental findings. The lubrication approximation was employed by Ho and Holland *et al* [14] and Greener and Middleman *et al* [15] for the theoretical analysis of reverse roll coating. They disregarded the presence of free surfaces, surface tension and dynamics of contact lines.

The innovative work based on roll coating was established by Greener and Middleman [16]. They developed a mathematical model through the hypothesis of small roll curvature and considered that both the roll and sheet move with similar speed. They employed lubrication approximation and obtained both the numerical and analytical solutions for Newtonian and non-Newtonian fluids. The reverse roll coating was also addressed by Hao and Haber [8]. They employed Galeriken finite element method for solution. Shiode *et al* [17] employed VOF to examine the reverse roll coating for flow simulations of dynamic wetting lines and concluded that the wetting lines reaches the nip as the speed ratio rises. Belblidia *et al* [18] established a model for reverse roll coating through Taylor-Galerkin pressure correction algorithm for maximum velocity. The modernization of the effort is inspired by the necessity in coating industry to coat steadily, rapidly and with undeviating thin sheets by enhancing the coater functioning conditions and coating rheology. Hao and Haber [8] developed the

Galeriken finite element technique for the analysis of coating flow of rotating reverse rolls. Zahid *et al* [19] investigated the second-grade materials for roll coating. They utilized the lubrication approximation theory (LAT) and obtained the numerical and graphical results for engineering parameters such as coating thickness, roller power input, pressure distribution, stress, split location, strength and temperature rise. Ali *et al* [20] analyzed the incompressible and non-isothermal viscoplastic fluid in the presence of magnetohydrodynamic (MHD) effects for reverse roll coating. They employed LAT for simplification of governing equations and analytic expressions for various engineering quantities have been obtained. The theoretical analysis of reverse roll coating for Williamson fluid was established by Ali *et al* [21]. The dimensionless governing equations were simplified through lubrication approximation. The perturbation technique was adopted to attain the analytic solution and concluded that the entailed material parameters allow a mechanism to control the pressure distribution, flow rate, coating thickness, power input and separation force. The non-Newtonian Jeffery fluid is investigated by Ali *et al* [22] in presence of MHD and heat transfer for reverse roll coating. They applied the LAT for simplification of governing equations and initiate that the coating thickness at the sheet reduces as the velocity ratios increases. Recently, Shahzad *et al* [23] proposed a theoretical analysis of non-isothermal couple stress fluid for reverse roll coating in presence of slip effects. They established the solution of governing equations by simplifying through LAT and employed shooting technique to obtain the solution. They found the decreasing tendency of flow rate for deviation of slip parameter. Mughees *et al* [24] investigated flow characteristics of couple stress fluid in blade coating using LAT. LAT is also employed by Kanwal *et al* [25] for analysis of blade coating process using simplified Phan-Thien-Tanner fluid model.

Numerous of researchers have examined non-Newtonian fluids as these fluids are extensively used in industries, scientific and engineering procedures such as crude oil extraction, geothermal and thermal insulation and aerodynamics. These fluids have composite rheological features. Distinct fluid models were inspected by researchers in accordance of certain material attributes such as Casson fluid, second-grade, third-grade, Oldroyd-B, couple stress and Jeffery fluid etc The under-consideration model is Jhonson-Segalman (JS) fluid model. The JS fluid entitles a non-monotonic association among the shear stress and shear rate in a shear flow for miscellaneous material parameters. It is a prime viscoelastic fluid model that can simulate shear thinning fluids. JS fluid enables non-affine deformations [26] and established by various researchers to illustrate the spurt phenomenon [27–29]. Spurt acquaint significant raise in volume to a negligible increase in driving pressure gradient. Three distinct JS fluid flows were investigated by Rao and Rajagopal [30]. The peristaltic transport of JS fluid with MHD was analyzed by Elshahed and Haroun [31] and employed the perturbation method to acquire the solution. JS fluid model was established by Hayat and Ali [32] by considering magnetic field in a circular tube. Asymmetric duct was considered by Hayat *et al* [33] for analysis of peristaltic flow of Jhonson-Segalman fluid. Peristaltic flow of JS fluid was inspected by Nadeem and Akbar [34] under consideration of heat transfer. They obtained the solution through perturbation and homotopy analysis method. The JS fluid in a tapering asymmetric canal is inspected by Kothandapni *et al* [35] that is caused by peristaltic stream train on inconsistent walls. They utilized perturbation technique to attain the solution of axial velocity, axial pressure gradient and stream function. The JS fluid model is established by Ashraf *et al* [36] for evaluation of peristaltic-cilia flow inside human fallopian tube for development of embryo. Recently, Kanwal *et al* [37] proposed JS fluid model for the analysis of blade coating and utilized LAT for simplification of governing equations. They adopted perturbation method for attaining the solution and concluded that the load decreases as Weissenberg number increases however coating thickness increases in comparison of viscous case.

According to literature review, there is no contribution of theoretical investigation of reverse roll coating for Jhonson-Segalman fluid model. The purpose of the contemporary work is to establish a mathematical model for the flow system of JS fluid in reverse roll coating and to investigate the effects of emerging parameters on fluid velocity, pressure gradient, coating thickness, pressure profile, roll separation force, power input and separation points.

2. Problem formulation

A two-dimensional, steady, incompressible flow of Jhonson-Segalman fluid is considered among two rolls that are rotating in the opposite directions as depicted in figure 1.

Where

- Peripheral velocities of rolls are supposed as U_f and U_r.
- The radius of each roll is R.
- U_f and U_r implies the forward and reverse rolls velocity respectively.

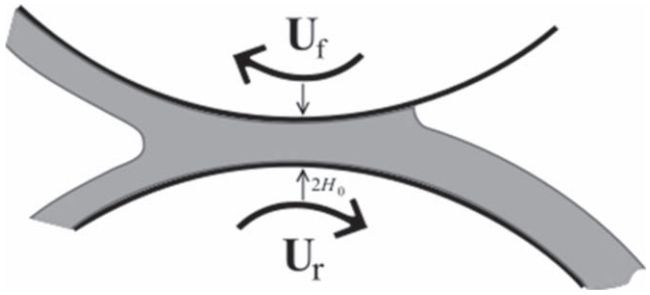

Figure 1. Geometry of the reverse roll coating.

- $k = \frac{U_r}{U_f}$ is ratio of velocities of both rolls that is uniform.
- $2H_0$ is gap among both rolls (nip region).
- x-axis is considered along flow movement however y-axis is taken transverse to the flow direction.

2.1. Basic equations

For an incompressible JS fluid with no body forces, the basic equations are as follows [38].

$$\text{div}\,\mathbf{V} = 0, \tag{1}$$

$$\text{div}\boldsymbol{\sigma} = \rho\frac{d\mathbf{V}}{dt} \tag{2}$$

For Jhonson-Segalman fluid, σ is defined as [37]

$$\boldsymbol{\sigma} = -P\mathbf{I} + \mathbf{T}, \tag{3}$$

$$\mathbf{T} = 2\mu\mathbf{D} + \mathbf{S}, \tag{4}$$

where

$$2\eta\mathbf{D} = \mathbf{S} + m\left[\mathbf{S}(\mathbf{W} - a\mathbf{D}) + \mathbf{S}(\mathbf{W} - a\mathbf{D})^t + \frac{d\mathbf{S}}{dt}\right], \tag{5}$$

and

$$\mathbf{D} = \frac{1}{2}[\mathbf{L} + \mathbf{L}^t], \tag{6}$$

$$\mathbf{W} = \frac{1}{2}[\mathbf{L} - \mathbf{L}^t], \tag{7}$$

$$\mathbf{L} = grad\ \mathbf{V}, \tag{8}$$

where

$\mathbf{V}$ = Velocity
ρ = Density of fluid
$\boldsymbol{\sigma}$ = Cauchy stress tensor
p = Pressure profile
$\mathbf{D}$ = Velocity gradient (symmetric part)
$\mathbf{W}$ = Velocity gradient (skew-symmetric part)
$\mathbf{I}$ = Identity tensor
$\mathbf{S}$ = Extra stress tensor
μ and η = Viscosities
a = Slip parameter
m = Relaxation time

If we take $a = 1$, the present model renovates to Oldroyd-B fluid model. For $\mu = 0$ and $a = 1$, JS fluid model converts to Maxwell fluid, and by considering $m = 0$ it transforms into Classical Navier–Stokes fluid model.

2.2. Governing equations and mathematical modelling

The velocity profile for the present situation is.

$$\mathbf{V} = [u(x, y), v(x, y)], \tag{9}$$

On account of equation (1), the component forms of equations (1) to (5) can be expressed as

$$\frac{\partial u}{\partial x} + \frac{\partial v}{\partial y} = 0, \tag{10}$$

$$\rho\left[u\frac{\partial u}{\partial x} + v\frac{\partial u}{\partial y}\right] = -\frac{\partial p}{\partial x} + \mu\left[\frac{\partial^2 u}{\partial x^2} + \frac{\partial^2 u}{\partial y^2}\right] + \frac{\partial S_{xx}}{\partial x} + \frac{\partial S_{xy}}{\partial y}, \tag{11}$$

$$\rho\left[u\frac{\partial v}{\partial x} + v\frac{\partial v}{\partial y}\right] = -\frac{\partial p}{\partial y} + \mu\left[\frac{\partial^2 v}{\partial x^2} + \frac{\partial^2 v}{\partial y^2}\right] + \frac{\partial S_{xy}}{\partial x} + \frac{\partial S_{yy}}{\partial y}, \tag{12}$$

$$\begin{aligned} 2\eta\frac{\partial u}{\partial x} &= S_{xx} + m\left[u\frac{\partial S_{xx}}{\partial x} + v\frac{\partial S_{xx}}{\partial y}\right] - 2amS_{xx}\frac{\partial u}{\partial x} \\ &+ m\left[(1-a)\frac{\partial v}{\partial x} - (1+a)\frac{\partial u}{\partial y}\right]S_{xy}, \end{aligned} \tag{13}$$

$$\begin{aligned} \eta\left[\frac{\partial u}{\partial y} + \frac{\partial v}{\partial x}\right] &= S_{xy} + m\begin{bmatrix} u\frac{\partial S_{xy}}{\partial x} \\ +v\frac{\partial S_{xy}}{\partial y}\end{bmatrix} + \frac{m}{2}\begin{bmatrix}(1-a)\frac{\partial u}{\partial y} \\ -(1+a)\frac{\partial v}{\partial x}\end{bmatrix}S_{xx} \\ &+ \frac{m}{2}\left[(1-a)\frac{\partial v}{\partial x} - (1+a)\frac{\partial u}{\partial y}\right]S_{yy}, \end{aligned} \tag{14}$$

$$\begin{aligned} 2\eta\frac{\partial v}{\partial y} &= S_{yy} + m\left[u\frac{\partial S_{yy}}{\partial x} + v\frac{\partial S_{yy}}{\partial y}\right] \\ &- 2amS_{yy}\frac{\partial v}{\partial y} + m\left[(1-a)\frac{\partial u}{\partial y} - (1+a)\frac{\partial v}{\partial x}\right]S_{xy}. \end{aligned} \tag{15}$$

These are the boundary conditions that will be considered for the problem under consideration[15]

$$\begin{cases} u = -U_r \ at \ y = \sigma, \\ u = U_f \ at \ y = -\sigma. \end{cases} \tag{16}$$

3. Dimensionless form

Introducing the suitable dimensionless parameters

$$\begin{aligned} &\bar{u} = \frac{u}{U}, \bar{x} = \frac{x}{L}, \bar{y} = \frac{y}{H_0}, \bar{h} = \frac{h}{H_0}, k = \frac{H_1}{H_0}, \\ &\bar{S} = \frac{H_0}{\mu U}S, L = \sqrt{2xR}, \bar{p} = \frac{pH_0^2}{(\eta+\mu)UL}. \end{aligned} \tag{17}$$

By using the above substitutions in equations (11) to (15), we get

$$\begin{aligned} \mathrm{Re}\in\left(u\frac{\partial u}{\partial x} + v\frac{\partial u}{\partial y}\right) &= -\left(\frac{\eta+\mu}{\mu}\right)\frac{\partial p}{\partial x} + \in^2\frac{\partial^2 u}{\partial x^2} \\ &+ \frac{\partial^2 u}{\partial y^2} + \in\frac{\partial S_{xx}}{\partial x} + \frac{\partial S_{xy}}{\partial y}, \end{aligned} \tag{18}$$

$$\begin{aligned} \mathrm{Re}\in^3\left(u\frac{\partial v}{\partial x} + v\frac{\partial v}{\partial y}\right) &= -\left(\frac{\eta+\mu}{\mu}\right)\frac{\partial p}{\partial y} + \\ \in^2\left(\in^2\frac{\partial^2 v}{\partial x^2} + \frac{\partial^2 v}{\partial y^2}\right) &+ \in^2\frac{\partial S_{xx}}{\partial x} + \in\frac{\partial S_{yy}}{\partial y}, \end{aligned} \tag{19}$$

$$\in\left(\frac{2\eta}{\mu}\right)\frac{\partial u}{\partial x} = S_{xx} + We \in \left(u\frac{\partial S_{xx}}{\partial x} + v\frac{\partial S_{xx}}{\partial y}\right)$$
$$- 2aWe \in S_{xx}\frac{\partial u}{\partial x} + We\begin{bmatrix} \in^2(1-a)\dfrac{\partial v}{\partial x} \\ -(1+a)\dfrac{\partial u}{\partial y}\end{bmatrix}S_{xy}, \tag{20}$$

$$\frac{\eta}{\mu}\left(\frac{\partial u}{\partial y} + \in\frac{\partial v}{\partial y}\right) = S_{xy} + We\begin{pmatrix} \in u\dfrac{\partial S_{xy}}{\partial x} \\ + \in v\dfrac{\partial S_{xy}}{\partial y}\end{pmatrix}$$
$$+ \frac{We}{2}\left[(1-a)\frac{\partial u}{\partial y} - (1+a)\frac{\partial v}{\partial x}\right]S_{xx}$$
$$+ \frac{We}{2}\left[\in^2(1-a)\frac{\partial v}{\partial x} - (1+a)\frac{\partial u}{\partial y}\right]S_{yy}, \tag{21}$$

$$\in\left(\frac{2\eta}{\mu}\right)\frac{\partial v}{\partial y} = S_{yy} + We\left[\in u\frac{\partial S_{yy}}{\partial x} + \in v\frac{\partial S_{yy}}{\partial y}\right]$$
$$- 2aWe \in S_{yy}\frac{\partial v}{\partial y} + We\begin{bmatrix}(1-a)\dfrac{\partial u}{\partial y} \\ -(1+a)\in\dfrac{\partial v}{\partial x}\end{bmatrix}S_{xy}, \tag{22}$$

where

$\mathrm{Re} = \frac{\rho U H_0}{\mu}$ Reynolds number.

$\in = \frac{H_0}{L}$ Ratio of height and length.

$We = \frac{mU}{H_0}$ Weissenberg number.

We begin with the LAT, which occurs in the reverse-roll coating process's nip region, where the most critical dynamic events occur. There is a small distance between the roll surfaces, which are nearly parallel and shift to either side for a short distance. Then it is reasonable to take up that $u << v$ and $\frac{\partial}{\partial x} << \frac{\partial}{\partial y}$. The fluid moves in the x-direction and the y-direction has no velocity. In consideration of this assumptions, the system of equations from (18) to (22) can be simplified as

$$-\left(\frac{\eta+\mu}{\mu}\right)\frac{\partial p}{\partial x} + \frac{\partial^2 u}{\partial y^2} + \frac{\partial S_{xy}}{\partial y} = 0, \tag{23}$$

$$\frac{\partial p}{\partial y} = 0, \tag{24}$$

$$We(1+a)\frac{\partial u}{\partial y}S_{xy} = S_{xx}, \tag{25}$$

$$S_{xy} + \frac{We}{2}(1-a)\frac{\partial u}{\partial y}S_{xx} - \frac{We}{2}(1+a)\frac{\partial u}{\partial y}S_{yy} = \left(\frac{\eta}{\mu}\right)\frac{\partial u}{\partial y}, \tag{26}$$

$$-We(1-a)\frac{\partial u}{\partial y}S_{xy} = S_{yy}. \tag{27}$$

One can notice from equation (24) that $p \neq p(y)$. By substituting equations (25) and (27) into equation (26), we obtain

$$S_{xy} = \frac{\left(\dfrac{\eta}{\mu}\right)\dfrac{\partial u}{\partial y}}{1 + We^2(1-a^2)\left(\dfrac{\partial u}{\partial y}\right)^2}, \tag{28}$$

By replacing equation (28) into (23), we get

$$\left(\frac{\eta+\mu}{\mu}\right)\frac{dp}{dx}=\frac{\partial^2 u}{\partial y^2}+\frac{\partial}{\partial y}\left[\frac{\left(\frac{\eta}{\mu}\right)\frac{\partial u}{\partial y}}{1+We^2(1-a^2)\left(\frac{\partial u}{\partial y}\right)}\right]. \tag{29}$$

By employing binomial expansion for small We^2, equation (29) takes the form

$$\frac{dp}{dx}=\frac{\partial}{\partial y}\left[\frac{\partial u}{\partial y}+We^2\beta\left(\frac{\partial u}{\partial y}\right)^3\right], \tag{30}$$

where $\beta=\frac{(a^2-1)\eta}{\eta+\mu}$.

The dimensionless boundary conditions for subjected to the problem are [15]

$$\begin{cases} u=1\ at\ y=-\sigma, \\ u=-k\ at\ y=\sigma. \end{cases} \tag{31}$$

4. Solution of the problem

It is of the utmost importance to be familiar with methods that can approximate the answers to different kinds of mathematical issues. This is due to the fact that the vast majority of mathematical problems do not have answers that can be stated explicitly. Asymptotic analysis is a powerful tool that, when combined with the perturbation technique, can be utilised to obtain approximations of solutions to difficult problems. This method can also be utilised alone. It is essential to make advantage of the structure of the problem when dealing with issues that include a parameter that is either extremely large or extremely small in order to produce the most accurate approximation. These methods are extremely helpful when dealing with converging and diverging geometries, such as coating flow problems [39, 40]. Due to the fact that equation (30) is a nonlinear differential equation, finding a solution in closed form can be challenging. Therefore, the solution of nonlinear differential equation given in equation (30) is obtained analytically by using regular perturbation technique for $We^2 << 1$ (as a parameter for perturbation) and expanding the velocity u, pressure p, pressure gradient $\frac{dp}{dx}$, and dimensionless film thickness in the power series of We^2

$$u=u_0+We^2u_1+We^4u_2..., \tag{32}$$

$$\frac{dp}{dx}=\frac{dp_0}{dx}+We^2\frac{dp_1}{dx}+We^4\frac{dp_2}{dx}..., \tag{33}$$

$$\lambda=\lambda_0+We^2\lambda_1+We^4\lambda_2..., \tag{34}$$

The terms u_0, $\frac{dp_0}{dx}$ and λ_0 are zeroth order solution and signifies the Newtonian case [15]. u_1, $\frac{dp_1}{dx}$ and λ_1 are first order terms and contributes the non-Newtonian effects. By replacing equations (32) and (33) into equation (30) and comparing alike powers of We^2, we acquire

For zeroth order $(We^2)^0$:

$$\frac{dp_0}{dx}=\frac{d}{dy}\left[\frac{du_0}{dy}\right], \tag{35}$$

$$\begin{cases} u_0=1\ at\ y=-\sigma, \\ u_0=-k\ at\ y=\sigma. \end{cases} \tag{36}$$

For first order $(We^2)^1$:

$$\frac{dp_1}{dx}=\frac{d^2u_1}{dy^2}+3\beta\left[\frac{du_0}{dy}\right]^2\left[\frac{d^2u_0}{dy^2}\right], \tag{37}$$

$$u_1=0\ at\ y=-\sigma,$$
$$u_1=0\ at\ y=\sigma. \tag{38}$$

The zeroth order solution for equations (35) and (36) can be obtained as

$$u_0=\frac{1}{2}[y^2-\sigma^2]\frac{dp_0}{dx}-\frac{1}{2\sigma}(k+1)y+\frac{1}{2}(1-k). \tag{39}$$

The dimensionless flow rate for zeroth order is [15]

$$\lambda_0 = \frac{1}{2}\int_{-\sigma}^{\sigma} u_0(y)\,dy, \tag{40}$$

By utilizing equations (39) and (40), we obtain

$$\frac{dp_0}{dx} = -\frac{3[(k-1)\sigma + 2\lambda_0]}{2\sigma^3}. \tag{41}$$

The zeroth order pressure can be attained by integrating equation (41) with $p_0 = 0$ as $x \to -\infty$

$$p_0(x) = \frac{1}{16(x^2+2)^2}\left[\begin{array}{l} -18\sqrt{2}\left\{\begin{array}{l}\lambda_0 + \\ \frac{2}{3}(k-1)\end{array}\right\}(x^2+2)^2 \\ \arctan\left(\frac{x\sqrt{2}}{2}\right) \\ -9\pi\sqrt{2}\left\{\begin{array}{l}\lambda_0 + \\ \frac{2}{3}(k-1)\end{array}\right\}(x^2+2)^2 \\ -36\left\{\begin{array}{l}\left(\lambda_0 + \frac{2}{3}(k-1)\right)x^2 \\ +\frac{10}{3}\lambda_0 + \frac{4}{3}(k-1)\end{array}\right\}x \end{array}\right]. \tag{42}$$

To acquire the coating thickness and pressure distribution, $\lambda_0(k)$ is needed therefore Swift-Stieber boundary condition is applied on pressure. It is assumed that the pressure and pressure gradient vanishes at the transition point $x = x_t$ (where lubrication type flow provides way to a transverse flow). By considering $\frac{dp_0}{dx} = 0$ in equation (41), we obtain.

$$\sigma_t = 1 + \frac{x_t^2}{2} = \frac{2\lambda_0}{1-k}, \tag{43}$$

we replace x by x_t in equation (42) and determine x_t in terms of λ_0 through equation (43) and substituting it into the subsequent equation gained from equation (42), the transcendental equation in λ_0 is attained. To tackle the complexity of this equation for evaluating λ_0, the Newton-raphson technique is applied with accuracy of 10^{-10} and predetermining various values of k.

It is similar to the zeroth order solution to have a solution of first order. By employing equation (35) into equation (39) and using boundary conditions of (38), we get.

$$u_1(y) = -\frac{1}{8\sigma^2}\left[3(y+\sigma)\left\{\begin{array}{l}\frac{2\beta\sigma^2\left(\begin{array}{l}\sigma^2 \\ +y^2\end{array}\right)\left(\frac{dp_0}{dx}\right)^3}{3} \\ -\frac{4y\beta\sigma(k+1)\left(\frac{dp_0}{dx}\right)^2}{3} \\ +\beta(k+1)^2\left(\frac{dp_0}{dx}\right) \\ -\frac{4\left(\frac{dp_1}{dx}\right)\sigma^2}{3}\end{array}\right\}(y-\sigma)\right]. \tag{44}$$

The dimensionless flow rate for first order is

$$\lambda_1 = \frac{1}{2}\int_{-\sigma}^{\sigma} u_1(y)\,dy, \tag{45}$$

From equations (42) and (43), we obtain

$$\frac{dp_1}{dx} = \frac{3(4\beta p^3\sigma^5 + 5\beta k^2 p\sigma + 10\beta k p\sigma + 5\beta p\sigma - 20\lambda)}{20\sigma^3}, \tag{46}$$

where $p = \frac{dp_0}{dx}$.

The expression for the first order pressure can be attained by integrating equation (46) with $p_1 = 0$ as $x \to -\infty$.

It is appealed that at the transition point $x = x_t$, Consequently, both pressure and its gradient vanish, and the lubricating type flow is transformed into a transverse type flow. By $\frac{dp_1}{dx} = 0$ in equation (45), we get

$$\lambda_1 = \frac{-3\beta(k\sigma + 2\lambda_0 - \sigma)\begin{bmatrix} 7k^2\sigma^2 + 18\lambda_0 k\sigma - 4k\sigma^2 \\ +18\lambda_0^2 - 18\lambda_0\sigma + 7\sigma^2 \end{bmatrix}}{20\sigma^4}. \tag{47}$$

The following is the definition of the simple second order material balance relationship for λ [15]

$$U_f H_f - U_r H_r = 2\lambda H_0 U_f, \tag{48}$$

and it may also result in the formation

$$\upsilon = \frac{H_f}{H_r} = 2\gamma\lambda + k, \tag{49}$$

where $\upsilon = \frac{H_f}{H_r}$ signifies the coating thickness. H_f and H_r represents the fluid sheet thickness on the forward and reverse rolls respectively. $\gamma = \frac{H_0}{H_r}$ indicates half of the nip region H_0 to entering fluid sheet H_r from the reverse roll therefore it is essential to identify $\lambda(k)$. We apply the Swift–Stieber boundary conditions to the pressure to determine the $\lambda(k)$ equation. In sight of the Swift–Stieber boundary condition for pressure, interchanging x with x_t in the resulting pressure equation and then plugging the value of λ into it all over the place in terms of x_t from equation (47), the transcendental equation in x_t is achieved. The Newton-Raphson method, which is a numerical method, is used to obtain results for the λ, which are presented in tables 3–4.

Up to first order, the perturbation solution is

$$\begin{cases} u &= u_0 + We^2 u_1, \\ \lambda &= \lambda_0 + We^2\lambda, \\ \dfrac{dp}{dx} &= \dfrac{dp_0}{dx} + We^2\dfrac{dp_1}{dx}. \end{cases} \tag{50}$$

5. Operating variables

When the pressure, pressure gradient, and velocity profile have been obtained, the required engineering parameters can be determined.

5.1. Separating force

The dimensionless separating force F of the rolls is [19]

$$F = \frac{\bar{F}H_0}{\mu_0 URW} = \int_{-\infty}^{x_t} p(x)\,dx, \tag{51}$$

where $\bar{F}$ signifies the non-dimensional roll separating force per unit width W.

5.2. Power input

The power transmitted through the roll to the fluid can be calculated by the integral [19]

$$p_w = \frac{\bar{P}}{\mu_0 WU^2} = \int_{-\infty}^{x_t} S_{xy}(x,\ 1)\,dx, \tag{52}$$

where p_w indicates the dimensional power. The dimensionless shear stress is

$$S_{xy} = \frac{\left(\dfrac{\eta}{\mu}\right)\dfrac{\partial u}{\partial y}}{1 + We^2(1 - a^2)\left(\dfrac{\partial u}{\partial y}\right)^2}. \tag{53}$$

6. Numerical solution

In this section, we offer a numerical solution for comparing equation (30), which was solved in the preceding section using the perturbation technique. Equation (30) is complex equation, it is difficult to solve this problem

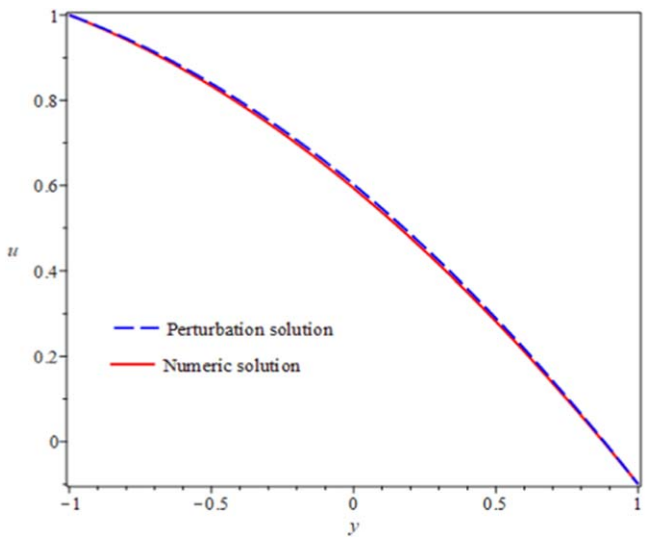

Figure 2. Compression between perturbation and numeric solution.

analytically, thus we must use a numerical technique to estimate the entire model. Here equation (30) is tackled via built-in maple command dsolve-numeric which is based on finite difference approach with Richardson extrapolation and is an appropriate, accurate method that can be used here.

We validate our numerical solution results by comparing them to the perturbation method results before moving on to the results and discussion. To this purpose, figure 2 is created, which depicts the velocity curve produced by numerical and analytical solutions. Numerical outcomes are shown by solid lines, whereas perturbed results are represented by dashed lines. This graph shows that both solutions have a strong association. This develops trust in both analytic and numerical solutions, as well as the outcomes projected by them. This clearly validates the validity of our numerical method.

The numerical calculations for velocity profile at different position during reverse roll coating process are performed for various involved material parameters such velocities ratio k and Weissenberg number We. Numerical results were highlighted through graphs and tables. All these numeric computations have been carried out at fixed value of pressure gradient $\frac{dp}{dx} = -0.3$ and $\beta = 0.5$.

The graphical solutions for velocity are shown in figures 3–6. The goal of this research is to use a numerical method to investigate the response of u to changes in k and We at various positions throughout the reverse roll coating procedure. It has been noticed that as k and we grow, fluid velocity decreases. Tables 1 and 2 show that the velocity reduces as one can moves away from the web at $\mathrm{x} = 0$.

7. Results and discussion

The major objective of this effort is to investigate the non-Newtonian JS fluid during reverse roll coating process theoretically and then validate results numerically. After changing to dimensionless form and employing appropriate dimensionless variables, the governing equations were solved using the analytical methodology perturbation method. The outcomes are graphically shown together with a discussion of the effects of various emergent characteristics on the flow system. Figures 7–10 illustrate the results of the non-dimensional velocity profiles at various points in the roll coating process for the different values of velocities ratio k and Weissenberg number We. Figures 11–14 show graphical representations of the pressure gradient and pressure distributions, while figures 15 and 16 show the relationship between the velocities ratio of the rolls, the Weissenberg number, and the coating thickness.

The variation in the non-dimensional velocity profile curves at the nip area is depicted in figure 7, whereas figure 8 are sketched at $x = 0.5$, for the increasing values of k in the selected domain of $[0.1, 0.9]$ by fixing $We = 0.5$ and $\beta = 0.5$. Where k is the ratio of the velocities of the reverse roll to those of the forward roll. It can be examined that velocity distribution declines by increasing the value of k. The maximum velocity was measured at the backward roller's roll surface, then it began to decrease as it moved towards the forward roll, eventually reaching zero when y belonged to a specific domain. Based on the value of k, it is possible to observe a reverse flow in the direction of the coating web after this domain. Figure 8 shows that the magnitude of the velocity increases as it approaches the separation point at various points in the reverse-roll coating process,

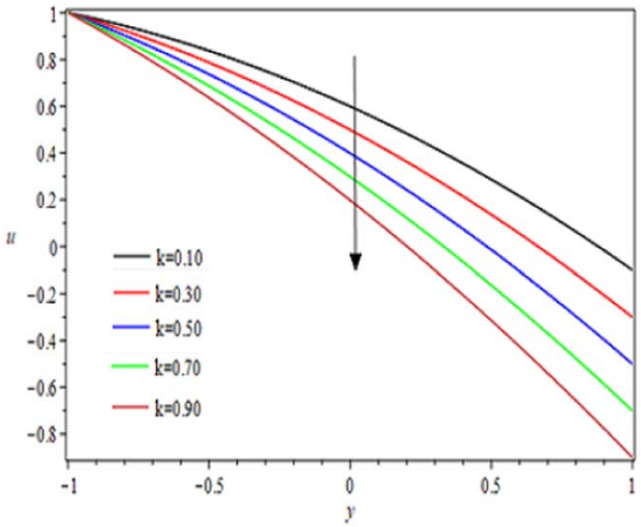

Figure 3. Effect of k on velocity at $x = 0$, when $We = 0.1$.

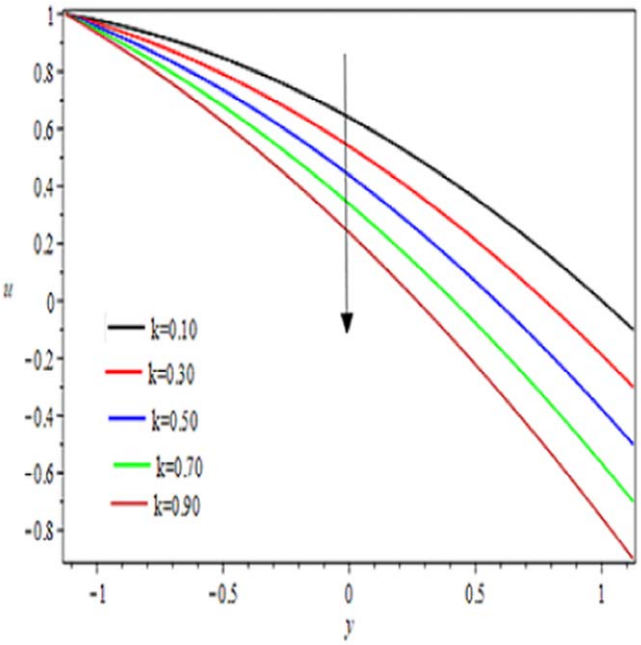

Figure 4. Effect of k on velocity at $x = 0.5$, when $We = 0.1$.

beyond the domain for y, where the velocity becomes zero, depending on the value of the k, and reaches its maximum speed at the roll's surface. Furthermore, it is discovered that for small k, the agreement with the model's predictions is quite good; however, as k approaches unity, the variances increase [15].

Figures 9–10 demonstrate the velocity distribution for numerous values of the Weissenberg number We at various locations ($x = 0$, $x = 0.5$) of the reverse roll coating process. The We is a dimensionless number that is used to assess flow velocity characteristics. It is worth noting that increasing the value of the We reduces the velocity profile. It is mathematically described as the ratio of viscous to the elastic forces. So for higher values of the We, viscous force becomes dominant that is higher viscous force causes a declination in flow velocity. One Can witnessed from figures 3–6 and 7–10 that, for small perturbation parameter We, we have a good agreement between all the two results.

Figures 11 and 12 show graphs of pressure gradient versus axial coordinate k. Figure 11 depicts the plots for various values of k while keeping the We constant throughout the computation, while figure 12 displays the plots for several values of k while maintaining the We constant. This graphic outcomes reveals the existence of

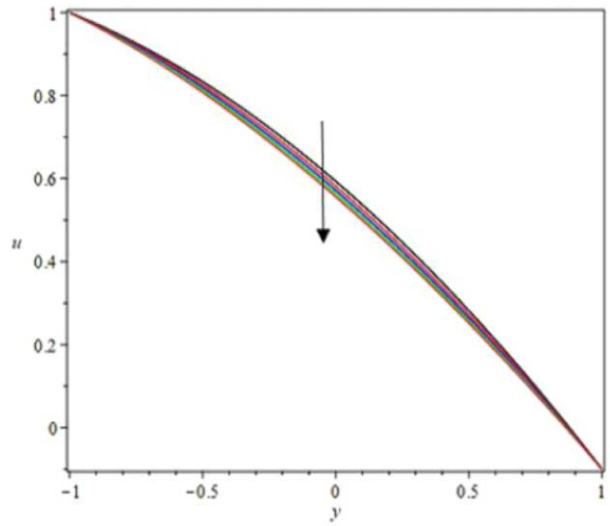

Figure 5. Effect of *We* on velocity at $x = 0$, when $k = 0.1$.

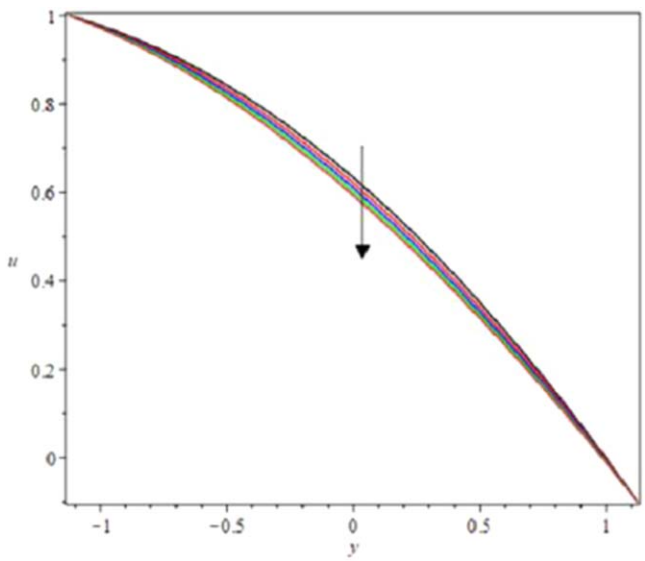

Figure 6. Effect of *We* on velocity at $x = 0.5$, when $k = 0.1$.

Table 1. Impact of *k* on velocity profile at k = 0.

y	$u_{k=0.1}$	$u_{k=0.2}$	$u_{k=0.3}$	$u_{k=0.4}$
−1	1	1	1	1
−0.8	0.94	0.93	0.92	0.91
−0.6	0.87	0.85	0.83	0.81
−0.4	0.79	0.76	0.73	0.70
−0.2	0.70	0.66	0.62	0.57
0	0.59	0.54	0.49	0.44
0.2	0.48	0.42	0.35	0.29
0.4	0.35	0.28	0.21	0.14

three separate zones, which are denoted as 'upstream,' 'nip region,' and 'downstream' respectively. The flow is resisted in the entrance and exit areas by the pressure gradient, but in the nip region it is assisted by the pressure gradient, which is due to the drag flow caused by the coater and substrate. Also, figure 11 show that the symmetric profiles around the nip area $x = 0$ can be determined. The absolute of the pressure gradient is

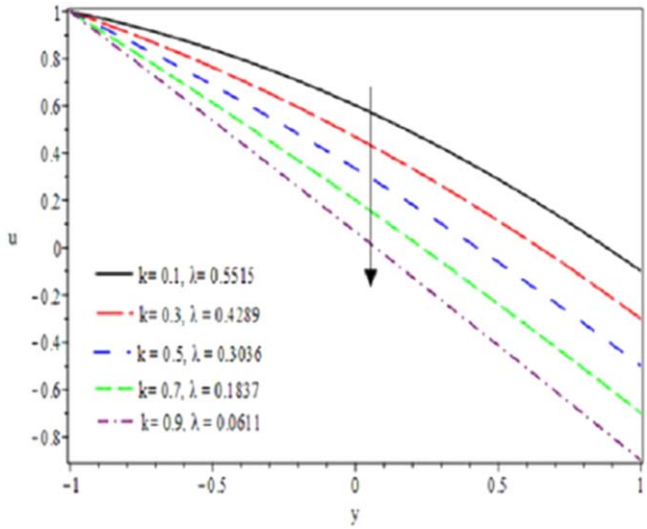

Figure 7. Effect of velocities ratio on velocity at $x = 0$.

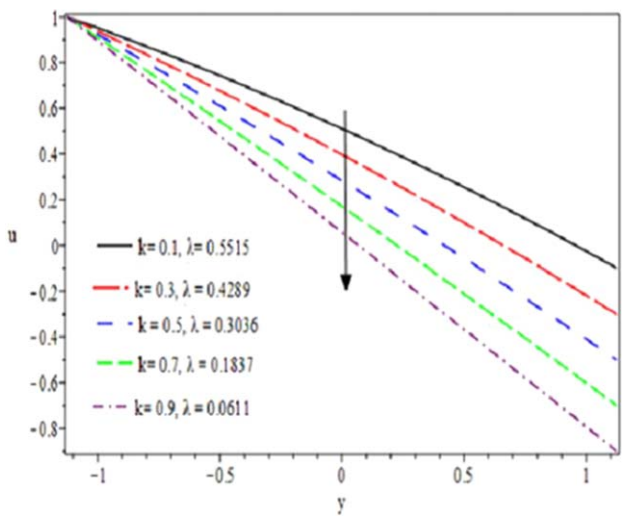

Figure 8. Effect of velocities ratio on velocity at $x = 0.5$.

Table 2. Impact of We on velocity profile at $x = 0$.

y	$u_{We=0.1}$	$u_{We=0.2}$	$u_{We=0.3}$	$u_{We=0.4}$
−1	1	1	1	1
−0.8	0.9421	0.9404	0.9387	0.9372
−0.6	0.8724	0.8691	0.8661	0.8632
−0.4	0.7910	0.7864	0.7822	0.7782
−0.2	0.6979	0.6924	0.6873	0.6825
0	0.5932	0.5871	0.5816	0.5765
0.2	0.4771	0.4709	0.4653	0.6503
0.4	0.3496	0.3439	0.3388	0.3343

greatest in the nip region, increasing symmetrically until it reaches its maximum value, then decreasing exponentially until it hits zero at detachment points. One can perceive that for a certain value of k, the pressure gradient decreases. Furthermore, it can be seen from figure 12 that the absolute value of pressure gradient increases with increasing We. It is further witnessed that the magnitude for pressure gradient of Newtonian fluid in the nip area is smaller than that of Johnson-Segalman fluid.

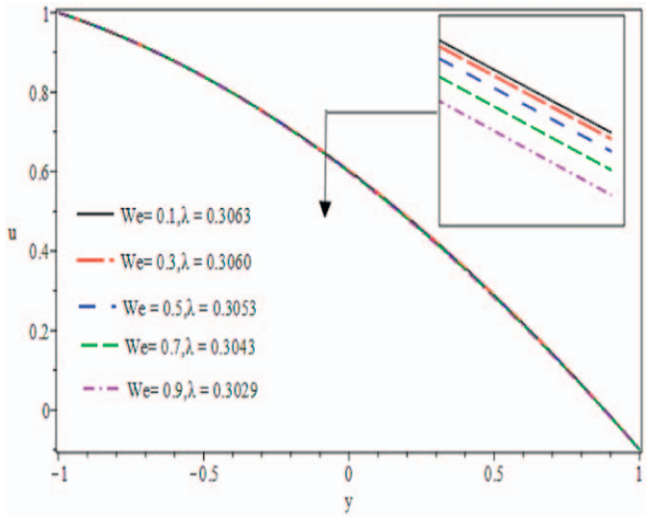

Figure 9. Effect of *We* on velocity at $x = 0$.

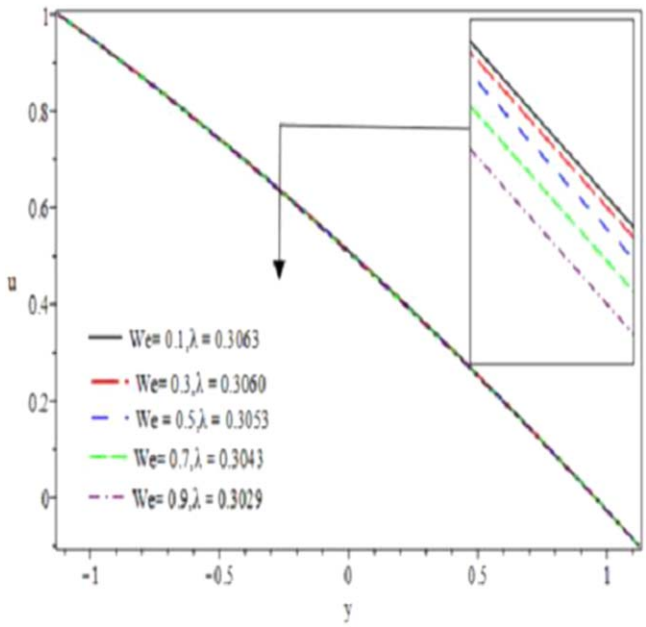

Figure 10. Effect of *We* on velocity at $x = 0.5$.

The graphical outcomes for the pressure distributions are presented in figures 13 and 14 for the various values of k and *We* respectively. Figure 13 shows that as one moves toward the negative x-axis, the pressure rises until it reaches its maximum near the roller's nip, and then begins to decline until the entry point of the sheet thickness is gotten. The pressure distribution is observed to decrease as the velocities ratio is increased. The pressure profiles versus x for various *We* are shown in figure 14. Due to the imposed boundary condition at the far upstream, all pressure profiles start at 0 in general. From this discussion, it is seen that at the attachment point the pressure is zero due to the imposed boundary condition, then it starts increasing while moving towards the nip region. Pressure gets its maximum values right before the nip region as shown in the figures, which is also true from a physical point of view. Then it starts decreasing and becomes zero at the separation point. This observation is very true from the physics of the problem that we need to have maximum pressure just right before the nip region in order to pass fluid flow through the narrow gap between two rolls rotating in opposite directions. When comparing the profiles of Newtonian and non-Newtonian viscoelastic fluids for various *We*, the Johnson-Segalman model predicts a greater magnitude of pressure than the Newtonian model.

Figures 15 and 16 show a graphical representation of the coating thickness versus the ratio of half of the nip region to the incoming fluid film for various k and *We*. It can be noticed that the coating thickness decreases as

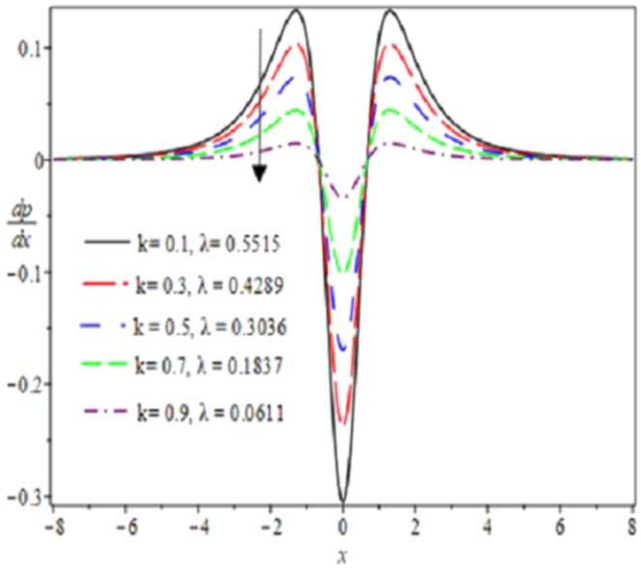

Figure 11. Effect of k on pressure gradient.

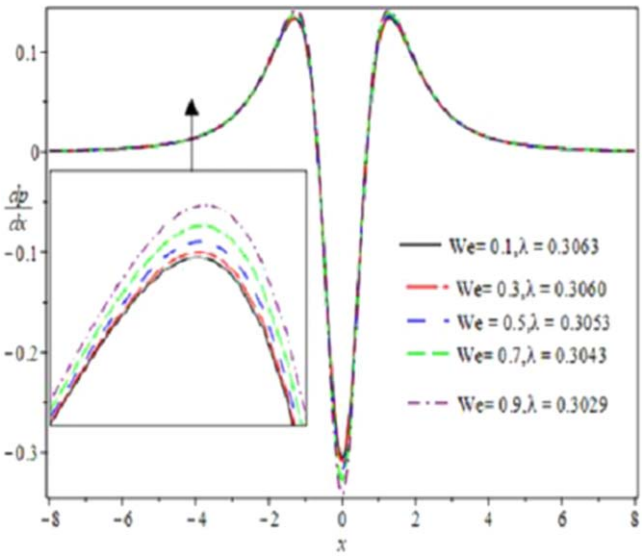

Figure 12. Effect of We on pressure gradient.

the k and We increase. This observation is also confirms through tables 3 and 4 where the volumetric flow rate and exit coating thickness are tabulated for various values of k and We.

Table 3 highlights the numerical consequences of the existing coating thickness υ, flow rate λ, separation point x_t, roll separation force F and power input p_w, which is developed using a k variation. Interestingly, table 1 has been presented to demonstrate how increasing the values of velocities ratio can reduce the flow rate, detachment point, coating thickness and roll separation force. The magnitude of power induced in the material by the rolls increases. Similar to this, table 4 demonstrates that an increase in the value of the We (assume $k = 0.1$) increases the magnitude of power input and roll separation force, while quantities of industrial interest, such as flow rate and coating thickness on the web, are decreased. The smallest coating thickness was recorded at $We = 0.9$, which is equal to 0.6240. It is interesting to note that roll-separating force has a direct effect on coating thickness and the flow rate. In fact, an increase in force decreases the thickness of coated layer onto a moving sheet. This observation is also confirms from table 4. When $We \rightarrow 0$ was set, the outcome was observed to be the same as the middleman [15] in the Newtonian scenario.

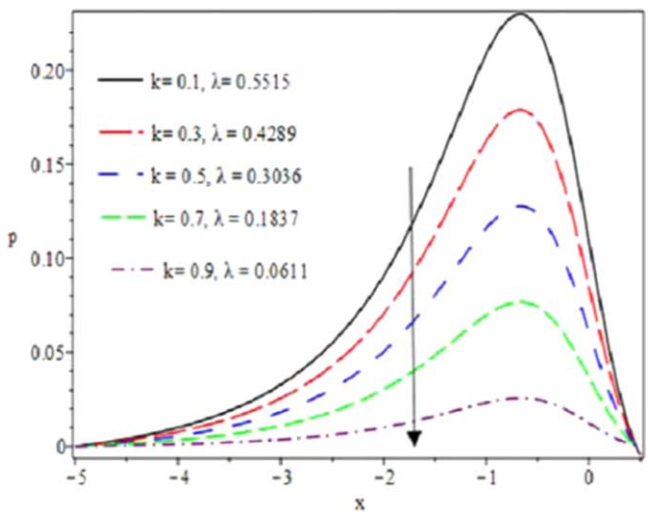

Figure 13. Effect of *k* on pressure distribution.

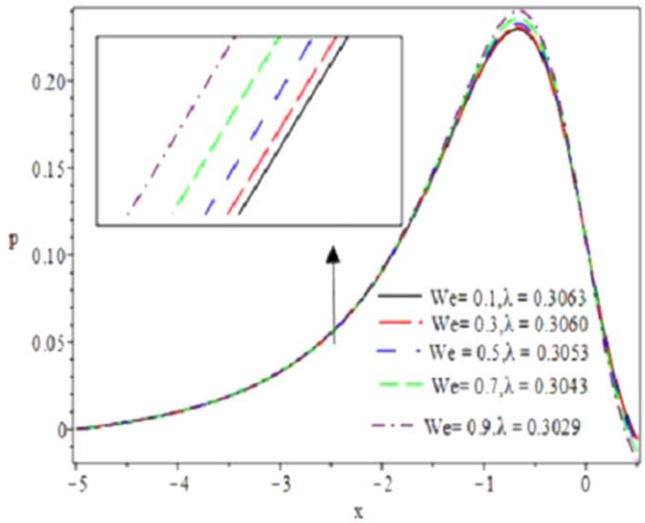

Figure 14. Effect of *We* on pressure distribution.

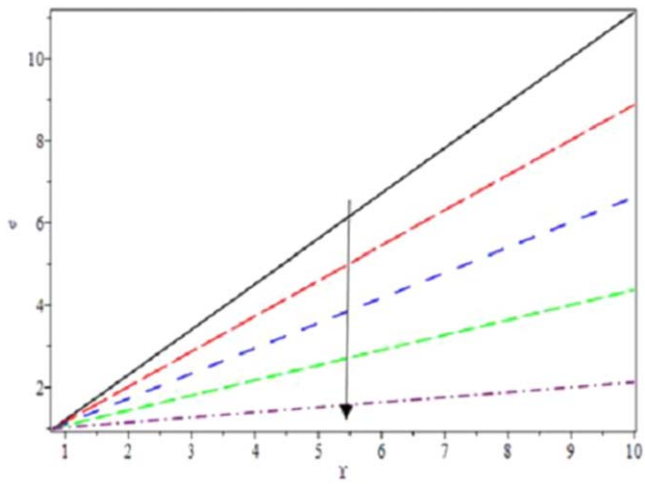

Figure 15. Effect of *k* on coating thickness.

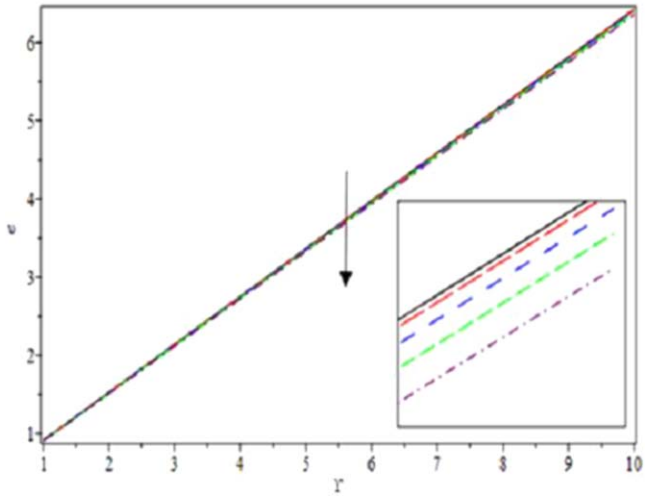

Figure 16. Effect of *We* on coating thickness.

Table 3. Influence of *k* on coating thickness, separation point, roll separation force and power input.

k	λ	x_t	υ	F	P_w
0.1	0.5515	0.9620	1.0927	0.2169	−1.1360
0.2	0.4902	0.9618	1.0823	0.1929	−1.2104
0.3	0.4289	0.9616	1.0720	0.1688	−1.2733
0.4	0.3676	0.9615	1.0616	0.1448	−1.3363
0.5	0.3063	0.9614	1.0513	0.1207	−1.3992
0.6	0.2451	0.9612	1.0411	0.0967	−1.4621
0.7	0.1837	0.9609	1.0306	0.0726	−1.5250
0.8	0.1224	0.9604	1.0203	0.0486	−1.5877
0.9	0.0611	0.9588	1.0099	0.0245	−1.6496

Table 4. Influence of *We* on flow rate, coating thickness, roll separation force and power input.

We	λ	υ	F	P_w
0.1	0.3060	0.6288	0.1945	−1.0455
0.2	0.3062	0.6286	0.1946	−1.0508
0.3	0.3060	0.6284	0.1948	−1.0594
0.4	0.3057	0.6279	0.1951	−1.0708
0.5	0.3053	0.6274	0.1955	−1.0845
0.6	0.3048	0.6267	0.1961	−1.09667.
0.7	0.3043	0.6260	0.1971	−1.1157
0.8	0.3037	0.6251	0.1986	−1.1319
0.9	0.3029	0.6240	0.2010	−1.1475

8. Concluding remarks

In the present work, the Lubrication Approximation Theory (LAT) was used along with the JS viscoelastic rheological model, in order to obtain analytical results as well as numerical results for the process of reverse roll coating fed from an infinite reservoir. The perturbation and numerical solutions for pressure, pressure gradient, velocity, flow rate, coating thickness, power input and separation points has been attained. Perturbation solutions up to $o(We^2)$ for the flow velocity presented and were compared to numerical solutions that were valid for small value of the velocities ratio and the Weissenberg number. It is found that, the fluid flow velocity is the decreasing function of velocities ratio and the maximum velocity of the fluid is at the surface of the roll. Further

it is noted that, as the Weissenberg number *We* rises, the fluid viscosity rises, and the fluid velocity falls. In the case of pressure and pressure gradient, they are decreasing functions of the velocities ratio, whereas, opposite trend was observed for the increasing values of *We*. Furthormore, when compared to the Newtonian model, the coating thickness reduces as the velocities ratio and *We* grow. It is observed that for small perturbation parameter *We*, we have a worthy agreement between all the two results, i.e., the perturbation, and the numerical solutions. Finally, when $We = 0$, we get the results presented by Middlemen [15] for Newtonian fluid.

Data availability statement

All data that support the findings of this study are included within the article (and any supplementary files).

Funding

This research article is funded by Natural Science Foundation of China (*NSFC*), grant number 11971378 and and by National Science, Research and Innovation Fund (*NSRF*), and King Mongkut's University of Technology North Bangkok with Contract no. KMUTNB-FF-65–24.

Conflicts of interest

The authors declare no conflicts of interest.

Future scope

Engineers and scientists of related industries from all over the world are welcomed to validate our results in a real environment on an experimental basis. Our study mainly emphasized the theoretical analysis of viscoelastic materials.

ORCID iDs

Fateh Ali https://orcid.org/0000-0003-4755-8370
Poom Kumam https://orcid.org/0000-0002-5463-4581

References

[1] Sweeting O J 1968 *The science and Technology Of polymer Films* (Interscience Publishers)
[2] Abbas Z, Naeem A and Khaliq S 2022 Variation in final sheet thickness in case of Sutterby fluid during the calendering process *J. Polym. Eng.* **42** 467–76
[3] Ellahi R, Zeeshan A, Hussain F and Abbas T 2018 Study of shiny film coating on multi-fluid flows of a rotating disk suspended with nano-sized silver and gold particles: a comparative analysis *Coatings.* **8** 422
[4] Balzarotti F and Rosen M 2009 Systematic study of coating systems with two rotating rolls *Latin American applied research.* **39** 99–104
[5] Ijaz N, Riaz A, Zeeshan A, Ellahi R and Sait S M 2020 Buoyancy driven flow with gas-liquid coatings of peristaltic bubbly flow in elastic walls *Coatings.* **10** 115
[6] Benkreira H, Edwards M and Wilkinson W 1981 A semi-empirical model of the forward roll coating flow of Newtonian fluids *Chem. Eng. Sci.* **36** 423–7
[7] Jang J-Y and Chen P-Y 2009 Reverse roll coating flow with non-newtonian fluids *Communications in Computational Physics.* **6** 536
[8] Hao Y and Haber S 1999 Reverse roll coating flow *Int. J. Numer. Methods Fluids* **30** 635–52
[9] Greener J, Sullivan T, Turner B and Middleman S 1980 Ribbing instability of a two-roll coater: Newtonian fluids *Chem. Eng. Commun.* **5** 73–83
[10] Coyle D, Macosko C and Scriven L 1990 Stability of symmetric film-splitting between counter-rotating cylinders *J. Fluid Mech.* **216** 437–58
[11] Chandio M and Webster M 2002 Numerical study of transient instabilities in reverse-roller coating flows *Int. J. Numer. Methods Heat Fluid Flow* **12** 375–403
[12] Coyle D, Macosko C and Scriven L 1990 The fluid dynamics of reverse roll coating *AlChE J.* **36** 161–74
[13] Hintermaier J and White R 1965 The splitting of a water film between rotating rolls *Tappi J.* **48** 617–25
[14] Ho W, Ws H and Fa H 1978 Between-rolls metering coating technique. a theoretical and experimental study *61 53–6* (https://pascal-francis.inist.fr/vibad/index.php?action=getRecordDetail&idt=PASCAL7860257561)
[15] Greener J and Middleman S 1981 Reverse roll coating of viscous and viscoelastic liquids *Industrial & Engineering Chemistry Fundamentals.* **20** 63–6
[16] Greener Y and Middleman S 1975 A theory of roll coating of viscous and viscoelastic fluids *Polymer Engineering & Science.* **15** 1–10
[17] Shiode H, Tamai H and Isaki T 2009 Flow simulations of dynamic wetting line at a reverse-roll coater using the VOF method *Nihon Reoroji Gakkaishi.* **37** 59–64

[18] Belblidia F, Tamaddon-Jahromi H, Echendu S and Webster M 2013 Reverse roll-coating flow: a computational investigation towards high-speed defect free coating *Mechanics of Time-Dependent Materials.* **17** 557–79
[19] Zahid M, Rana M and Siddiqui A 2018 Roll coating analysis of a second-grade material *J. Plast. Film Sheeting* **34** 232–55
[20] Ali F, Hou Y, Zahid M and Rana M A 2020 Theoretical study of the reverse roll coating of non-isothermal magnetohydrodynamics viscoplastic fluid *Coatings.* **10** 940
[21] Ali F, Hou Y, Zahid M and Rana M A 2020 Mathematical analysis of pseudoplastic polymers during reverse roll-coating *Polymers.* **12** 2285
[22] Ali F, Hou Y, Zahid M, Rana M and Usman M 2022 Influence of magnetohydrodynamics and heat transfer on the reverse roll coating of a Jeffrey fluid: a theoretical study *J. Plast. Film Sheeting* **38** 72–104
[23] Shahzad H, Wang X, Hafeez M B, Shah Z and Alshehri A M 2021 Study of slip effects in reverse roll coating process using non-isothermal couple stress fluid *Coatings.* **11** 1249
[24] Mughees M, Sajid M, Ali N and Shahzad H 2020 Nonisothermal analysis of a couple stress fluid in blade coating process *Polymer Engineering & Science.* **60** 1129–37
[25] Khaliq S and Abbas Z 2021 Theoretical analysis of blade coating process using simplified Phan-Thien-Tanner fluid model: an analytical study *Polymer Engineering & Science.* **61** 301–13
[26] Johnson M Jr and Segalman D 1977 A model for viscoelastic fluid behavior which allows non-affine deformation *J. Non-Newtonian Fluid Mech.* **2** 255–70
[27] Kolkka R, Malkus D, Hansen M and Ierley G 1988 Spurt phenomena of the johnson-segalman fluid and related models *J. Non-Newtonian Fluid Mech.* **29** 303–35
[28] Malkus D S, Nohel J A and Plohr B J 1990 Dynamics of shear flow of a non-newtonian fluid *J. Comput. Phys.* **87** 464–87
[29] McLeish T and Ball R 1986 A molecular approach to the spurt effect in polymer melt flow *J. Polym. Sci., Part B: Polym. Phys.* **24** 1735–45
[30] Rao I and Rajagopal K 1999 Some simple flows of a johnson-segalman fluid *Acta Mech.* **132** 209–19
[31] Elshahed M and Haroun M H 2005 Peristaltic transport of johnson-segalman fluid under effect of a magnetic field *Mathematical Problems in Engineering.* **2005** 663–77
[32] Hayat T and Ali N 2007 A mathematical description of peristaltic hydromagnetic flow in a tube *Appl. Math. Comput.* **188** 1491–502
[33] Hayat T, Afsar A and Ali N 2008 Peristaltic transport of a Johnson–Segalman fluid in an asymmetric channel *Math. Comput. Modell.* **47** 380–400
[34] Nadeem S and Akbar N S 2009 Influence of heat transfer on a peristaltic flow of Johnson Segalman fluid in a non uniform tube *Int. Commun. Heat Mass Transfer* **36** 1050–9
[35] Kothandapani M, Prakash J and Pushparaj V 2016 Nonlinear peristaltic motion of a Johnson–Segalman fluid in a tapered asymmetric channel *Alexandria Engineering Journal.* **55** 1607–18
[36] Ashraf H, Siddiqui A and Rana M 2018 Analysis of the peristaltic-ciliary flow of Johnson–Segalman fluid induced by peristalsis-cilia of the human fallopian tube *Math. Biosci.* **300** 64–75
[37] Kanwal M, Wang X, Shahzad H, Sajid M and Yiqi C 2021 Mathematical modeling of Johnson-Segalman fluid in blade coating process *J. Plast. Film Sheeting* **37** 463–89
[38] Yasmin H, Hayat T, Alsaedi A and Alsulami H 2014 Peristaltic flow of Johnson-Segalman fluid in asymmetric channel with convective boundary conditions *Applied Mathematics and Mechanics.* **35** 697–716
[39] Khaliq S and Abbas Z 2021 Analysis of calendering process of non-isothermal flow of non-Newtonian fluid: a perturbative and numerical study *J. Plast. Film Sheeting* **37** 338–66
[40] Javed M A, Nasir S, Ali N and Arshad S 2022 Mathematical simulation of the calendering process for non-Newtonian polymers *J. Plast. Film Sheeting* 87560879211066900 (https://doi.org/10.1177/87560879211066900)